

# Enhancing millimeter-wave communication: a tropical perspective on raindrop size distribution and signal attenuation

Nurul Najwa Md Yusof<sup>1,2</sup>, Jafri Din<sup>1</sup>, Lam Hong Yin<sup>3</sup>

<sup>1</sup>Department of Communication Engineering, Faculty of Electrical Engineering, Universiti Teknologi Malaysia, Johor Bahru, Malaysia

<sup>2</sup>Department of Polytechnic and Community College Education, Ministry of Higher Education, Putrajaya, Malaysia

<sup>3</sup>Department of Electrical Engineering, Faculty of Engineering Technology, Universiti Tun Hussein Onn Malaysia, Parit Raja, Malaysia

## Article Info

### Article history:

Received Apr 18, 2024

Revised Sep 17, 2024

Accepted Oct 1, 2024

### Keywords:

Millimeter-wave

Raindrop size distribution

Specific attenuation

Supervised machine learning

Tropical monsoons

## ABSTRACT

This study tackles rain attenuation in millimeter-wave (mm-wave) communication, a critical concern for the advancement of 5G wireless technology. It examines the variability of raindrop size distribution (DSD) and its impact on specific attenuation, with a focus on tropical environments such as Malaysia. Using the Joss-Waldvogel disdrometer, this study collected and analyzed extensive DSD data over three years, revealing that the highest DSD concentrations do not necessarily result in the greatest specific attenuation. This study adopted a machine learning approach, specifically supervised learning with linear regression, to enhance the accuracy of attenuation prediction models. A new set of coefficients for the power-law model of specific attenuation was derived and benchmarked against the ITU-R P.838-3 standard and similar studies in comparable climates. The findings emphasize the importance of developing region-specific models that consider local meteorological variations, potentially offering significant improvements to the reliability and design of mm-wave communication systems in the future.

*This is an open access article under the [CC BY-SA](https://creativecommons.org/licenses/by-sa/4.0/) license.*



## Corresponding Author:

Jafri Din

Department of Communication Engineering, Faculty of Electrical Engineering, Universiti Teknologi Malaysia

81310 UTM Johor Bahru, Johor Darul Ta'zim, Malaysia

Email: jafri@utm.my

## 1. INTRODUCTION

The demand for more communication channels that can accommodate faster data rates and broader bandwidths has led to the research of the millimeter-wave (mm-wave) spectrum, which typically operates above 20 GHz, with wavelengths less than 10 mm [1]. However, the promise of unprecedented data transmission speeds and network reliability is tempered by the physical limitations imposed by the atmosphere, particularly through rain attenuation. Rain attenuation plays a crucial role in the deterioration of mm-wave signals [2], [3] by causing deep fades that impact the availability of the link [4], thus becoming a formidable challenge to maintaining the integrity of high-frequency signal transmissions over considerable distances. Rain attenuation depends heavily on local climatology [5]. Previous works have highlighted the significant impact of raindrop size distribution (DSD) on rain attenuation. For example, several studies have emphasized that the empirical model provided by ITU-R does not have local rain characteristics [6], [7]. The ITU-R model may be effective for lower frequencies, but as the frequency moves into the mm-wave range, the ITU-R model begins to lose accuracy [8]. This limitation was acknowledged in [9] that suggested the ITU-R model's inadequacy is due to not accounting for local meteorological variations, necessitating a more detailed understanding of DSD [8]. The coefficient of the power-law in specific attenuation is significantly

influenced by the local raindrop size distribution (DSD), which can differ across various regions [10]. This importance was corroborated in [11] which stated that specific attenuation progressively relies on the DSD at higher frequencies. Most studies examining rain attenuation, including those conducted by ITU-R, have primarily concentrated on temperate regions [12]. However, the characteristics and structures of rainfall events in tropical areas differ significantly, leading to inaccurate predictions for tropical climates [13].

The influence of DSD on mm-wave propagation is crucial in tropical regions due to the rain's unique characteristics, such as high rainfall rates and intense precipitation events with larger raindrops, which cause greater scattering and absorption of electromagnetic waves, resulting in higher attenuation [14]. This significantly degrades the performance of communication systems, particularly 5G and 6G networks [15]. Because ITU-R frequently underestimates specific attenuation, some studies have highlighted the importance of region-specific adjustments and more complex modeling techniques [16], [17]. For example, the variability of DSD in India revealed that the specific rain attenuation at 100 GHz decreases less with increasing rain rates than at 60 GHz [18]. Another significant work by Alonge [19] analyzed the effects of rainfall attenuation across different regions in Africa, indicating the impact of climatic and geographic factors on DSD patterns. These studies emphasized the importance of considering regional DSD variations in attenuation modeling and improving the accuracy of rainfall attenuation forecasts, thereby contributing to the development and optimization of robust communications systems that can withstand the severe weather conditions typical of these areas [9].

This research addresses the deficiencies in accurately predicting rain attenuation due to the oversight of regional meteorological fluctuations by existing models in tropical countries such as Malaysia. This is done by amassing and extensively scrutinizing three years of DSD data utilizing the Joss-Waldvogel disdrometer. By developing new coefficients for a power-law model for specific attenuation using supervised machine learning and comparing them with the ITU-R P.838-3 standard, this study strives to refine the attenuation prediction model, capturing seasonal and weather-related variations. Additionally, it investigates the impact of different rain types and intensities on specific attenuation across various mm-wave frequencies.

This paper is organized as follows: section 2 describes the key features of the Joss-Waldvogel RD-69 disdrometer, including its operational principle, sensing area, and calibration methods. Section 3 explains the calculation of specific attenuation ( $\gamma$ ) using the ITU-R P.838-3 standard and the T-matrix method, which considers complex scattering patterns of raindrops, as well as the specific attenuation results for frequencies in the range 18 to 38 GHz, highlighting the variations between different rain types and comparing the new power-law model coefficients with the ITU-R standard. This section also provides complementary cumulative distribution function (CCDF) for different rain events, accenting the differences observed during the southwest (SW) and northeast (NE) monsoons. Finally, Section 4 concludes the study by summarizing the results and suggesting possible improvements for mm-wave communication systems in tropical regions.

## 2. METHOD

In this study, DSD was measured using Joss Waldvogel disdrometer, particularly the RD-69 model, which was located at Universiti Teknologi Malaysia in Kuala Lumpur (UTM, KL). It operates on the principle of detecting droplets passing through a sensing area and sorting them into 20 different channels based on their size and fall velocity. The RD-69 disdrometer consists of a conical Styrofoam collector that is positioned above a sensing unit. The collector is intended to minimize the effects of wind and to ensure that raindrops fall vertically onto the sensor. Meanwhile, the sensing unit comprises a coil of wire that is suspended in a magnetic field [20]. When a raindrop strikes the collector, it exerts force and pushes the coil. This movement generates a voltage in the coil, which is amplified and recorded by a data logger. The DSD is derived from the voltage pulses produced by the RD-69 disdrometer. The pulse amplitude corresponds to the size of the causing raindrop. To calculate the DSD, the count of pulses for each size category is divided by the sampling period, yielding the DSD in units of mm/h. The measurement setup for the disdrometer is shown in Figure 1. The details of the measurement setup can be found in [21].

The sampling area for the RD-69 disdrometer is  $S = 5000 \text{ mm}^2$  with a one-minute integration time of  $T = 60 \text{ s}$  and diameter classes ranging between 0.3 and 5.3 mm. The rain rate (mm/h) given by the disdrometer can be calculated using (1):

$$R = \frac{3600\pi}{65T} \sum_{i=1}^{20} D_i^3 n_i \quad (1)$$

where  $D_i$  is the diameter of the  $i$ th bin with the number of raindrops,  $n_i$ . The measured DSD in ( $\text{m}^{-3}\text{mm}^{-1}$ ) can be expressed by (2) where  $v(D_i)$  is the Gunn-Kinzer velocity of raindrops in still air [22], [23] and  $\Delta D_i$  is the span of class  $i$ th bin determined by the disdrometer.

$$N(D_i) = \frac{n_i}{v(D_i) \times S \times T \times \Delta D_i} \tag{2}$$

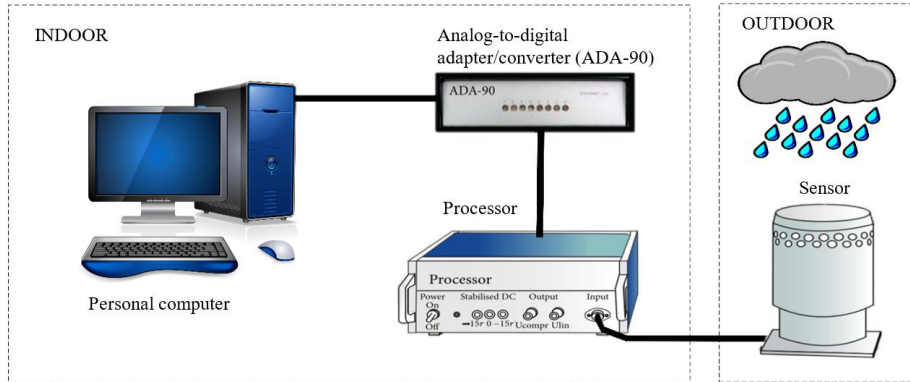


Figure 1. Joss-Waldvogel RD-69 disdrometer measurement setup [24]

This study analyzes 36 months of DSD data from the RD-69 disdrometer, which provided raw datasets encompassing 61,384 rainy minutes (1-minute integration time). From these data, 556 rain events were identified, with each event separated by dry periods of a minimum duration of one hour, separating each event from the subsequent event. The events were classified based on their intensity and duration into three categories: drizzle, shower, and thunderstorm, based on previous studies [25], [26]. Drizzle occurrences are characterized by rain rates below 20 mm/h that last for a minimum of 10 consecutive minutes, while showers exhibit rain rates ranging from 20 to 70 mm/h sustained for 10 consecutive minutes. Thunderstorm events are identified by rain rates exceeding 70 mm/h sustained for at least 5 consecutive minutes. Events with rain rates below 5 mm/h at the start and end were not included. The bin number with its corresponding mean drop diameter is presented in Table 1. The summary of average measured drop counts for SW and NE monsoons at 3:00-6:00 am and 3:00-6:00 pm during thunderstorm, shower and drizzle events were also given in the same table.

Table 1. Summary of average measured raindrops during thunderstorm events in the SW and NE monsoon

Bin Number	Mean diameter (mm)	SW		NE		SW		NE		SW		NE	
		Thunderstorm		Thunderstorm		Shower		Shower		Drizzle		Drizzle	
		AM	PM	AM	PM	AM	PM	AM	PM	AM	PM	AM	PM
1	0.36	0	0	0	0	0	0	0	0	0	0	0	0
2	0.46	1	0	1	0	2	1	0	0	3	1	0	1
3	0.55	11	6	5	6	10	8	11	11	19	5	3	6
4	0.66	39	20	21	18	37	19	65	27	23	17	12	25
5	0.77	53	39	56	39	61	34	105	44	34	29	29	40
6	0.91	151	133	224	132	174	106	249	137	77	116	102	137
7	1.12	250	223	331	228	252	181	348	249	134	202	215	256
8	1.33	196	164	215	174	186	146	229	176	107	156	200	209
9	1.51	141	124	149	128	140	106	163	131	80	109	133	148
10	1.67	131	115	129	112	121	97	139	120	83	94	118	132
11	1.91	214	177	195	163	188	148	230	187	132	136	190	199
12	2.26	156	130	139	120	156	107	178	131	106	101	156	125
13	2.58	75	67	70	63	73	57	65	66	53	55	75	63
14	2.87	48	45	40	43	45	40	42	43	33	39	40	41
15	3.20	34	40	32	38	34	34	34	31	26	33	35	31
16	3.54	14	18	19	20	15	20	13	15	13	19	12	14
17	3.92	9	12	11	14	8	14	9	11	17	15	8	10
18	4.35	2	5	5	7	2	7	4	6	8	9	5	6
19	4.86	1	2	2	3	1	5	1	4	9	5	1	4
20	5.30	0	1	0	0	0	2	0	1	2	2	1	1

**2.1. Determination of southwest and northeast monsoon in Malaysia**

Malaysia, a tropical country located at 4.2105° N, 101.9758° E, comprises a peninsular and the island of Borneo, which includes Sabah and Sarawak. It experiences two main monsoon seasons: the Southwest (SW) monsoon from late May to September and the Northeast (NE) monsoon from November to

March, with a transitional inter-monsoon period in between. Wind speed and direction data, which are important for identifying these monsoons, were obtained from the Malaysian Meteorological Department (MET), Visual Crossing, and the National Oceanic and Atmospheric Administration (NOAA). During the NE monsoon, the region experiences the strongest winds, with average speeds reaching up to 15.4 m/s [27] whereas the SW monsoon features lower wind speeds, averaging around 2.0 to 5.2 m/s, which resulting in calmer sea conditions [28]. Despite the difference in wind speeds, a study reported that in Peninsular Malaysia, wind speed does not significantly influence wind direction, irrespective of its origin [29]. The study also revealed that the wind direction exhibits greater stability in the eastern region of Peninsular Malaysia compared to the western part. This suggests a tendency for wind direction to vary more during the southwest SW monsoon than the northeast NE monsoon.

The JW RD-69 disdrometer was installed at the Universiti Teknologi Malaysia in Kuala Lumpur (UTM, KL) in the southwest of Peninsular Malaysia. Specific wind speed and direction data are not available for this location. The nearest weather stations are in Petaling Jaya and Subang, according to MET and NOAA records. Meteorologically, the wind direction is determined via the place of origin of the wind [30]. Figure 2 shows a simplified wind rose diagram to help better understand wind direction. A decade-long statistical analysis found that the wind direction during the SW monsoon in Subang from 1999 to 2007 varied between 197 and 231 degrees, while it varied between 170 and 211 degrees at Kuala Lumpur International Airport (KLIA) [29]. Further investigation revealed that during the NE monsoon at KLIA from 2014 to 2019, the wind direction varied between 11 and 339 degrees, peaking in 2018, while other years experienced directions between 11 and 46 degrees [31]. During the SW monsoon, the direction fluctuated between 172 and 212 degrees. Kamisan *et al.* [32] showed a circular distribution pattern of wind direction during the SW monsoon at four locations in Melaka, Senai, Alor Setar and Langkawi were between 90 and 315 degrees. Melaka, which is the closest to UTM, KL, particularly showed wind directions between 150 and 285 degrees. Therefore, this study assumes that the wind directions during the SW monsoon are between 180 and 270 degrees and between 0 and 90 degrees during the NE monsoon.

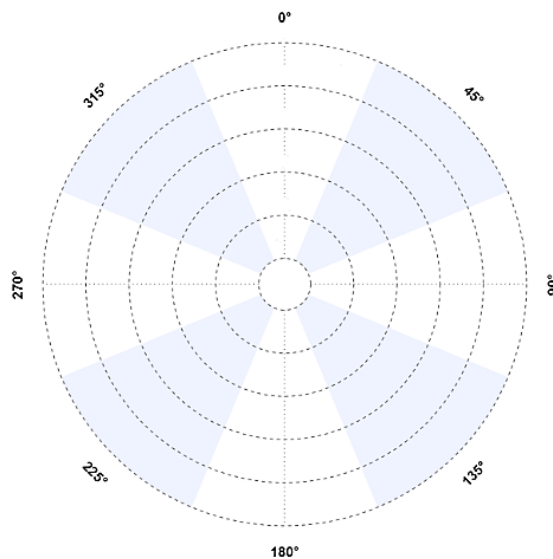


Figure 2. Wind rose diagram

## 2.2. Specific attenuation calculations

The specific attenuation,  $\gamma$ , quantifies the reduction in signal strength per unit length caused by rain, assuming a constant rate of rainfall along the entire path of signal propagation [33]. It is a critical parameter in understanding the impact of rainfall on signal propagation. In this study,  $\gamma$  was computed using two distinct methods. First, the ITU-R P.838-3 standard [34], which provides a widely accepted framework for estimating specific attenuation based on the rain rate and frequency using the expression (3):

$$\gamma = kR^\alpha \quad (3)$$

where  $k$  and  $\alpha$  are coefficients that vary based on polarization and frequency.

Besides the ITU-R P.838-3 model, specific attenuation can be calculated by incorporating the forward-scattering amplitude (FSA) into the formula. The T-matrix method, an advanced computational approach, is employed to determine the FSA. This method accounts for complex scattering patterns and provides a detailed evaluation of how electromagnetic waves interact with raindrops, especially where traditional techniques like point matching might fall short [35]. The T-matrix method is useful for analyzing scattered waves from non-spherical raindrops and is also reliable for various drop shapes and radio frequencies [36], [37]. In this study, the FSA is calculated using a Python implementation for T-matrix scattering calculations provided by Leinonen [38], assuming raindrops are oblate spheroids with a defined axial ratio. The formula for specific attenuation in dB/km is presented in (4):

$$\gamma_{H,V} = 8.686 \times 10^3 \times \lambda \times \sum_{i=1}^{20} \text{Im}(f_{H,V}(D_i)) \cdot N(D_i) \cdot \Delta D_i \quad (4)$$

where  $\lambda$  represents the wavelength in meters,  $m(f_{H,V}(D_i))$  denotes the imaginary component known as the FSA in meters,  $N(D_i)$  is the count of drops per unit volume per unit diameter of drop and  $\Delta D_i$  specifies the interval of drop size in millimeters.

### 3. RESULTS AND DISCUSSION

The results are presented in this section. Subsection 3.1 presents comparison of the diurnal variations between SW and NE monsoons for thunderstorm events. Subsection 3.2 provides specific attenuations over different frequencies ranging from 8 to 48 GHz for different types of precipitation with comparison to the ITU-R P.838-3. Subsection 3.3 shows the derived  $k$  and  $\alpha$  using supervised machine learning, along with the complementary cumulative distribution function of the specific attenuations computed using the derived coefficients.

#### 3.1. Diurnal variations in raindrop size distribution during monsoon events

A comparison of SW and NE monsoon thunderstorm events observed between 3:00 and 6:00 pm local time with rain rates between 55 and 75 mm/h provides interesting insights into DSD and its effects on specific attenuation mm-wave frequencies. Figure 3 shows an analysis of six sample events from the SW monsoon in Figure 3(a) and the NE monsoon in Figure 3(b), revealing that the maximum DSD concentration does not necessarily result in the highest specific attenuation. For both monsoons, bin 12 consistently showed the highest specific attenuation with measurements of 0.96, 1.66, and 3.24 dB/km during the SW monsoon, and slightly reduced values of 0.89, 1.53, and 2.98 dB/km during the NE monsoon at 18, 26, and 38 GHz frequencies. The cumulative specific attenuation for all bins exhibited similar trends with overall values of 6.33, 11.35, and 17.44 dB/km for the SW monsoon compared to 6.37, 11.30, and 17.08 dB/km for the NE monsoon. These minor variations are quantified as 0.04, 0.05, and 0.36 dB/km for the frequencies under study. It was also observed that the DSD concentration in bin 12 was lower during both monsoons, with  $172.48 \text{ m}^{-3} \text{ mm}^{-1}$  and  $158.62 \text{ m}^{-3} \text{ mm}^{-1}$  for SW and NE monsoons, in stark contrast to the peak concentrations found in bin 7, which reached  $735.81 \text{ m}^{-3} \text{ mm}^{-1}$  and  $753.89 \text{ m}^{-3} \text{ mm}^{-1}$ .

The same parameters were measured for both the SW monsoon and the NE monsoon, as illustrated in Figure 4. Figure 4(a) shows the measurements for the SW monsoon during the morning between 3:00 and 6:00 a.m., while Figure 4(b) presents the corresponding measurements for the NE monsoon during the same period. However, the results were limited by the rarity of the events, resulting in only two sample events being analyzed for each monsoon. Despite the limited data, the study highlights the consistent observation that the denser DSD is not associated with greater specific attenuation. Focusing on bin 12, the analysis revealed that the highest specific attenuation values are 1.15, 1.99, and 3.88 dB/km for the SW monsoon and 1.03, 1.77, and 3.45 dB/km for the NE monsoon at 18, 26, and 38 GHz, respectively. The aggregate specific attenuation values for all bins were 6.07, 11.35, and 18.51 dB/km for the SW monsoon, compared to 6.31, 11.49, and 18.34 dB/km for the NE monsoon. Slight variations between these monsoon periods are 0.24, 0.14, and 0.17 dB/km for the three frequencies examined. Furthermore, it was noticed that in bin 12, the DSD concentration only reached  $206.64 \text{ m}^{-3} \text{ mm}^{-1}$  for the SW monsoon and  $183.75 \text{ m}^{-3} \text{ mm}^{-1}$  for the NE monsoon. This contrasts with the peak concentrations observed in bin 7, where values were recorded at  $824.93 \text{ m}^{-3} \text{ mm}^{-1}$  and  $1092.75 \text{ m}^{-3} \text{ mm}^{-1}$ .

The results indicate that during the diurnal variations for both monsoons, bins with the highest number of raindrops do not necessarily lead to the greatest attenuation due to increased FSA from larger raindrop particles [39]. In this study, the greatest attenuation was caused by raindrop diameters ranging between 1.91 mm and 3.20 mm. Similar results were reported in Durban where critical raindrop diameters contributing most to specific attenuation were found to be in the range of 1.0 to 3.0 mm for convective rain, which includes thunderstorm rain [40]. A more recent study in the same area had slightly different results where

the specific attenuation peaked between 1.4 and 2.7 mm for frequencies between 10 to 100 GHz [41]. The influence of raindrop diameter on attenuation was also evident in the findings from Rwanda where the largest contributions to specific attenuation were from drop diameters in the range of 1.5 to 3.5 mm [42].

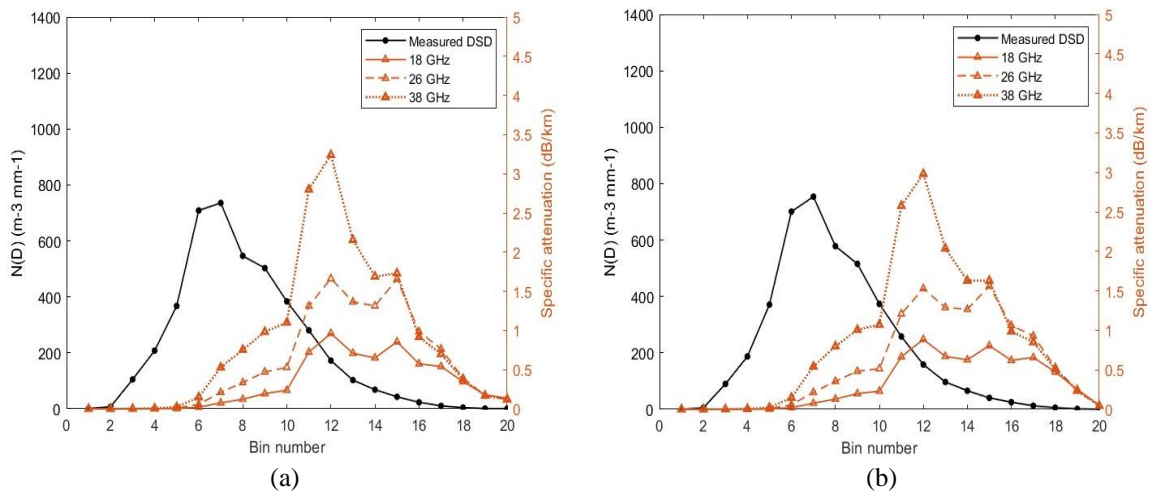


Figure 3. Measured DSD and specific attenuation at different frequencies (18, 26, and 38 GHz) during thunderstorm events observed between 3:00-6:00 pm with rain rates of 55-75 mm/h during (a) SW monsoon and (b) NE monsoon

Field studies have confirmed that raindrops, particularly those around 1 mm in diameter, begin to oscillate due to eddy shedding, which significantly alters their shape and thus their scattering characteristics. Observations of forward scatter over long paths have demonstrated that rain can significantly increase signal levels, with larger drops contributing more to this effect due to their greater scattering cross-sections [43]. Additionally, theoretical analyses showed that the forward scattering intensity is sensitive to the particle diameter, with larger particles exhibiting more pronounced scattering effects [44]. Taken together, these results highlight that raindrop diameter plays a critical role in determining forward scattering amplitude, with larger drops causing stronger scattering effects due to their larger size, oscillations, and internal structural variations.

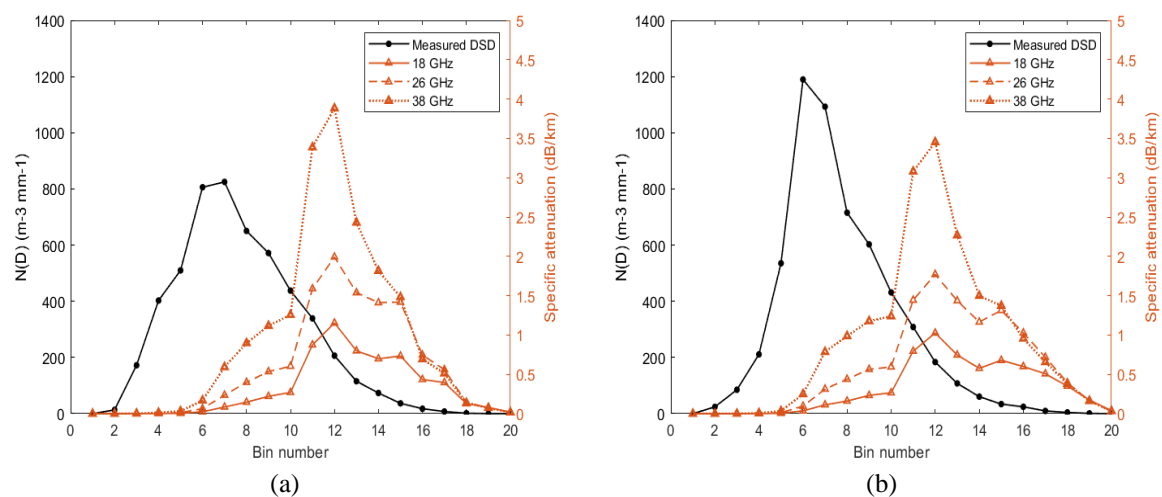


Figure 4. Measured DSD and specific attenuation at different frequencies (18, 26, and 38 GHz) during thunderstorm events observed between 3:00-6:00 am with rain rates of 55-75 mm/h during (a) SW monsoon and (b) NE monsoon

**3.2. Specific attenuation for different rain types across frequencies**

Figures 5 and Figures 6 highlight significant differences in specific attenuation values for various rain types during the SW monsoon, illustrated in Figures 5(a) and 6(a), and the NE monsoons, illustrated in Figures 5(b) and 6(b). The figures illustrate how the measured specific attenuation for drizzle, shower, and thunderstorm deviates from the ITU-R model across a frequency range from 8 to 48 GHz. Measurements were taken between 3:00-6:00 pm and 3:00-6:00 am, with rainfall rates ranging from 55 to 75 mm/h. Specific attenuation increases with frequency for all conditions, a common trend due to higher frequency rain attenuation.

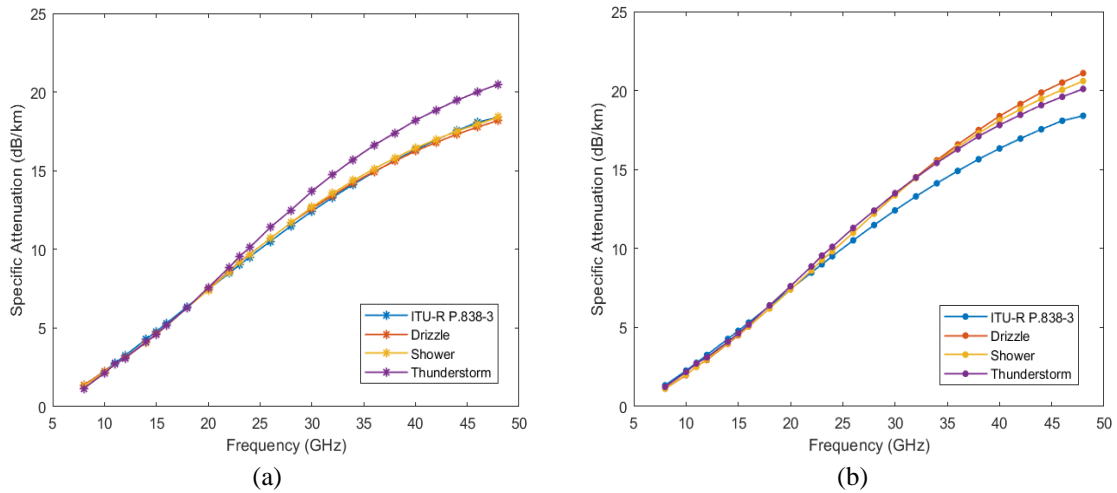


Figure 5. Comparison of specific attenuation for different rain types against ITU-R P.838-3 predictions during (a) SW monsoon and (b) NE monsoon between 3:00 to 6:00 pm

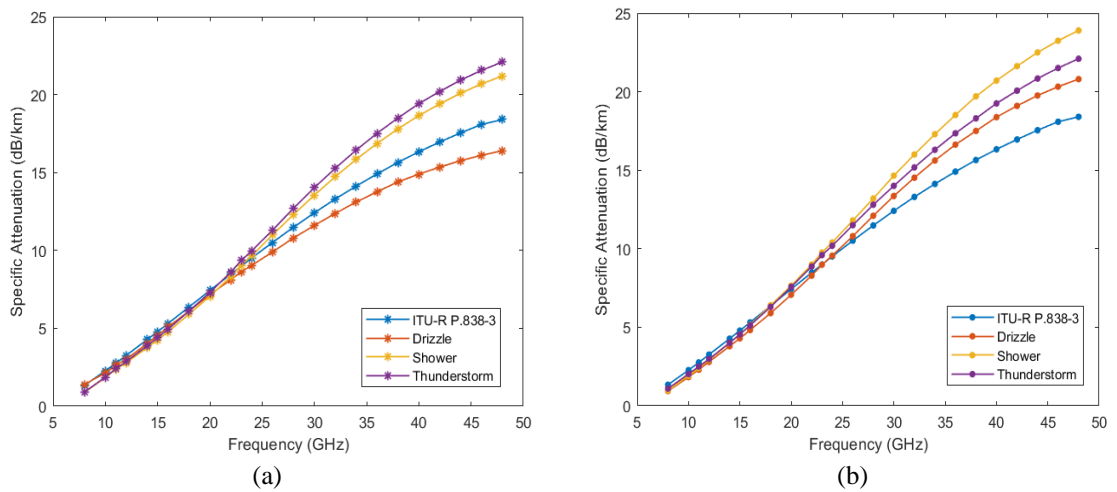


Figure 6. Comparison of specific attenuation for different rain types against ITU-R P.838-3 predictions during (a) SW monsoon and (b) NE monsoon between 3:00 to 6:00 am

In the evening, during the SW monsoon, drizzle and shower closely follow the ITU-R model, suggesting its reliability for these rain types. For instance, at 38 GHz, specific attenuation is 15.6 dB/km for drizzle and 15.8 dB/km for shower, aligning with ITU-R predictions. However, thunderstorm shows specific attenuation at 17.4 dB/km which is higher than the model estimates, likely due to larger raindrops. In the NE monsoon, discrepancies with the ITU-R model become pronounced above 30 GHz, with specific attenuation values for drizzle, shower, and thunderstorm are 17.5, 17.3, and 17.1 dB/km respectively, exceeding model predictions. Morning specific attenuation varies more significantly than in the afternoon. During the SW monsoon, observed values are 14.4 dB/km for drizzle, 17.8 dB/km for showers, and 18.5 dB/km for

thunderstorm, proving the underestimation of the ITU-R model. In the NE monsoon, the values are 17.5 dB/km for drizzle, 19.7 dB/km showers, and 18.3 dB/km for thunderstorm, also surpassing model predictions. Some of these differences are larger than 2 dB/km, which can significantly impact the design of wireless communication systems, requiring adjustments in power margins or link distances to maintain signal quality [45].

The results reveal that the NE monsoon exhibits higher specific attenuation for all rain types, whereas the SW monsoon shows a mixed pattern, with attenuation values that are sometimes higher, lower, or closely following the ITU-R model. This may be due to the NE monsoon contributing more rainfall across Peninsular Malaysia than the SW monsoon, coupled with the fact that most areas in Peninsular Malaysia have become drier during the SW monsoon over the last three decades [46]. In comparison, a study in Gadanki [47] found that the DSD during the SW monsoon has more large drops and fewer small drops compared to the NE monsoon, which has more small drops and fewer large drops, especially at low rain rates. Larger raindrops cause higher attenuation, resulting in higher attenuation during SW monsoon compared to NE monsoon, contrary to this study's observations.

The diurnal and seasonal variations in DSD are also evident in other tropical locations like Singapore and Kototabang, where local convection and ocean-land contrasts significantly influence rainfall characteristics [48]. In Singapore, the variations in DSD are less pronounced compared to Gadanki and Kototabang. This stability in DSD is attributed to Singapore's unique position, influenced by both land and oceanic rainfall, resulting in more stable rainfall patterns throughout the year. Conversely, Kototabang exhibits significant diurnal variations in DSD, influenced by ocean-land contrast and mountain effects that generate local convection, especially in the afternoon. During both the SW and NE monsoons, Kototabang experiences notable changes in DSD, leading to variations in raindrop sizes and rainfall intensity.

It is expected that this study will show how the ITU-R P.838 model underestimates specific attenuation in regions with significant diurnal and seasonal variations. The results confirm this and show higher attenuation values than predicted by the ITU-R model, especially during heavy rainfall events such as thunderstorms and showers in both the SW and NE monsoons. These observed variations in DSD and precipitation characteristics highlight the complexity and regional specificity of tropical precipitation and suggest that local model adjustments may be required to capture the nuances of monsoon rainfall in tropical regions.

### 3.3. Derivation of $k$ and $\alpha$ using supervised machine learning

Supervised machine learning (SML) significantly improves rain attenuation prediction models by leveraging historical data to identify patterns and relationships that traditional statistical models may overlook. As mentioned before, the model recommended by the ITU-R often relies on complex mathematical formulations and empirical data that may not generalize well across different climatic zones, particularly in regions with heavy rainfall like the tropics [49], [50]. SML models can be trained using locally measured data, increasing their adaptability and effectiveness for specific regions. For instance, a machine learning model trained on seven years of rainfall data in Nigeria outperformed the ITU-R model in predicting rain attenuation, with a lower root-mean-square (RMSE) [49]. Similarly, a neural network model has proven to be more effective than the empirical power-law approach, leading to a considerable reduction in the mean square error [51].

Using SML in rain attenuation prediction is not limited to simple neural networks; more complex architectures like convolutional neural networks (CNNs) have also been employed. For example, a CNN trained on large amounts of data from commercial microwave links could detect rainfall-specific attenuation patterns with reasonable accuracy and reducing falsely estimated rainfall [52]. The adaptability of SML models enables the incorporation of various input parameters, such as path length, operating frequency, wave polarization, and rain rate distribution. This feature enables them to discover hidden connections and enhance prediction without the need for complex mathematical expressions [53], making SML a valuable tool in the ongoing effort to improve rain attenuation predictions and mitigate the adverse effects of weather on communication systems.

In this study, the SML approach with linear regression was used to derive  $k$  and  $\alpha$  values for specific attenuation for different rain types at 38 GHz frequency during the SW and NE monsoons. A set making up 80% of training data and 20% of test data was used to validate the machine learning model's performance. The SML algorithm was implemented using Python, and the code was written in a Jupyter Notebook from Anaconda Navigator. The resulting values are presented in Table 2 alongside the statistical method for comparison, together with their corresponding R-squared and RMSE values. Notably, the differences between SML and statistical method-derived  $k$  and  $\alpha$  are relatively small, with high R-squared values indicating good fits for both methods.



These minor differences between the SML and statistical method derived coefficients suggest that the linear regression model has effectively captured the underlying relationships within the data, which the statistical method has traditionally approximated. This also indicates that the machine learning approach does not significantly overfit despite its complexity, and the model is well-tuned with a properly sized dataset [45]. The consistency between established models is further validated by comparing the  $k$  and  $\alpha$  values with findings from Alhilali *et al.* [54] and Lam *et al.* [55], whose studies were conducted in Johor Bahru and Kuala Lumpur, Malaysia, correspondingly. It is important to note, however, that these studies did not categorize precipitation by rain types. Figure 7 displays the diurnal variations of the CCDF to assess the influence of raindrop size distribution on mm-wave propagation at 38 GHz at separate times under different monsoon conditions using the same sets of samples as in section 3.1. Figures 7(a) and 7(b) present the CCDFs for drizzle during the early morning (3:00 to 6:00 a.m.) and late afternoon (3:00 to 6:00 p.m.), respectively. Figures 7(c) and 7(d) illustrate the results for shower conditions during the same time periods, while Figures 7(e) and 7(f) depict the CCDFs for thunderstorms, again comparing the early morning with the late afternoon, respectively. These figures also compare predictions from ITU-R P.838-3 together with [54] and [55]. The CCDFs incorporate data points for drizzle, shower, and thunderstorm conditions, using  $k$  and  $\alpha$  coefficients derived using SML as outlined in Table 2.

Table 2. Coefficient of  $k$  and  $\alpha$  at 38 GHz

		Rain Type	$k$	$\alpha$	$R^2$	RMSE
Southwest monsoon	Statistical method	Drizzle	0.27933	1.01685	0.99058	0.75917
		Shower	0.30097	0.97304	0.9872	0.96499
		Thunderstorm	0.29235	0.98425	0.99282	1.19772
	SML	Drizzle	0.27897	1.01678	0.99193	0.80678
		Shower	0.29961	0.97386	0.98454	0.92712
		Thunderstorm	0.29152	0.98469	0.99250	1.13874
Northeast monsoon	Statistical method	Drizzle	0.27816	1.03249	0.99296	0.72578
		Shower	0.29047	0.00521	0.99214	0.83533
		Thunderstorm	0.28855	0.9938	0.99306	1.20399
	SML	Drizzle	0.27765	1.03288	0.99309	0.56209
		Shower	0.29699	0.99543	0.99077	0.95248
		Thunderstorm	0.28988	0.99279	0.99285	1.16387
	Alhilali <i>et al.</i> [54]	-	0.40000	0.93500	0.99700	-
	Lam <i>et al.</i> [55]	-	0.35250	0.94820	0.98200	-

These plots, juxtaposed with the ITU-R P.838-3 model, show that all rain types, including those studied in [54], [55], consistently register above the ITU-R line. These discrepancies highlight the ITU-R model's temperate bias, which may not accurately capture the more pronounced rain-induced attenuation at higher frequencies characteristic of tropical regions with heavy rainfall and high-water content clouds [50], [56]. The physical basis of the ITU-R model, which aims to maximize accordance with experimental data, also faces challenges in tropical regions because of the unique atmospheric conditions, which are not fully accounted for in the model [57]. Additionally, the frequent high winds in tropical areas may not be adequately addressed by the model, leading to potential underestimation of attenuation [15]. Studies from Malaysia and Ota, Nigeria, have highlighted the inadequacy of ITU-R models in these regions, where existing models underestimated the attenuation margins required for reliable communication [58], [59]. These studies emphasize the need for new models that better predict rain attenuation in tropical climates. Experimental studies in tropical locations also highlighted the combined effects of rain and wind on signal attenuation, suggesting that the ITU-R model could be supplemented with additional models to account for these factors [15].

The derived  $k$  and  $\alpha$  coefficients in this study are tailored to the specific conditions measured, potentially providing improved accuracy of specific attenuation than the standard ITU-R model. Significant differences between these machine learning-based predictions and the ITU-R model may indicate the need for regional or condition-specific enhancements to rain attenuation predictions. Specific attenuation, especially in the mm-wave frequencies, has substantial consequences for signal propagation. Overestimation can lead to conservative system designs, whereas underestimation may result in failures under adverse conditions [60].

The observation of dB/km variations within the CCDF curves plays a role in shaping the system's link margin. This directly impacts key design choices regarding transmitter power settings, antenna gain selections, and the establishment of suitable fade margins. In millimeter-wave propagation, even minor differences can have a noticeable impact on link budget design and system reliability [15]. The dB/km discrepancies in the CCDF curves are critical for determining link margins and defining system

characteristics, such as transmitter power and fade margins. This is relevant for communication systems operating within frequencies susceptible to rain attenuation, requiring the use of adaptive methods to ensure consistent service quality.

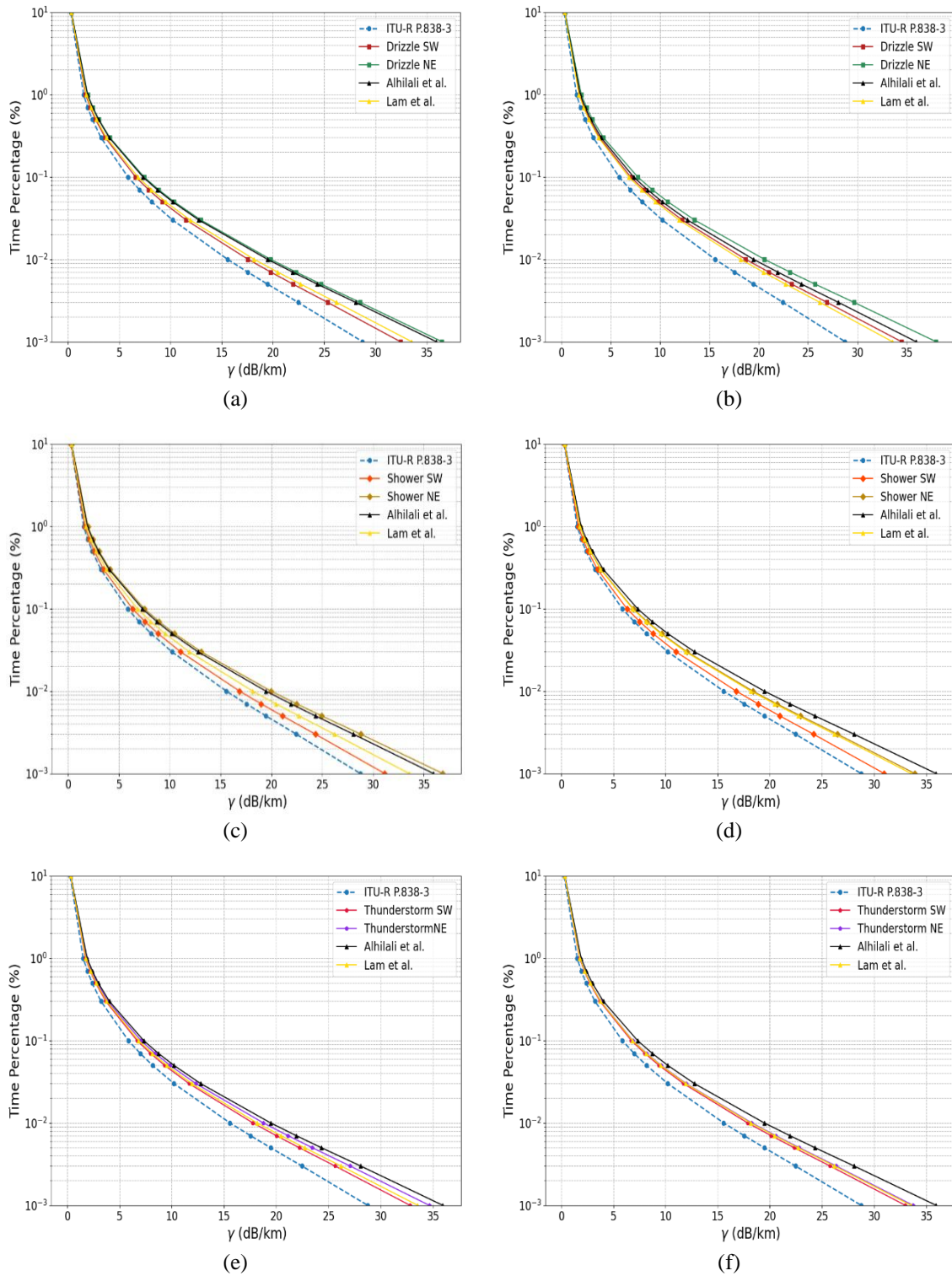


Figure 7. Time percentage occurrences at 38 GHz, represented by specific attenuation ( $\gamma$ ) values across different rain types and times: (a) Drizzle, 3:00 to 6:00 am, (b) Drizzle, 3:00 to 6:00 pm, (c) Shower, 3:00 to 6:00 am, (d) Shower, 3:00 to 6:00 pm, (e) Thunderstorm, 3:00 to 6:00 am, and (f) Thunderstorm, 3:00 to 6:00 pm

#### 4. CONCLUSION

This study has validated the crucial importance of rain attenuation in millimeter-wave communication systems and its significant variability attributed to DSD, especially in regions with tropical climates like Malaysia. By examining a three-year dataset of extensive DSD information obtained from the Joss-Waldvogel disdrometer, the observation shows that the distribution of DSD does not exhibit a linear relationship with the intensity of specific attenuation. The application of SML with linear regression led to the development of enhanced attenuation prediction models, yielding a new set of power-law coefficients. These coefficients show marked improvement over the standard ITU-R P.838-3 model, suggesting that machine learning (ML) methods can capture the nuances of local rain attenuation more effectively. The findings align with the expectations set forth in the introduction, confirming that region-specific models are essential for accurately predicting rain attenuation in tropical climates. Furthermore, this study also shows that the reliability of mm-wave communication systems is greatly improved by incorporating local meteorological variations into attenuation models. Future studies could concentrate on refining these ML models with larger datasets and exploring the application of other advanced regression algorithms. Additionally, the integration of these findings into the design and optimization of wireless network infrastructure holds great promise for improving the resilience of communication systems against the challenges posed by tropical weather patterns.

#### REFERENCES




- [1] S. J. Seah, S. L. Jong, H. Y. Lam, and J. Din, "Rain fade margin of terrestrial line-of-sight (LOS) links for 5G networks in Peninsular Malaysia," *International Journal of Microwave and Wireless Technologies*, vol. 14, no. 6, pp. 750–760, Jul. 2022, doi: 10.1017/S1759078721000751.
- [2] I. Mata-Alonso, J. Manuel Riera, D. Pimienta-del-Valle, and A. Benarroch, "Rain attenuation of millimeter waves investigated from drop size distributions," in *2023 17th European Conference on Antennas and Propagation (EuCAP)*, Mar. 2023, pp. 1–5, doi: 10.23919/EuCAP57121.2023.10133385.
- [3] L. Li, A. Sali, and S. Q. Wali, "Attenuation of mmWave based on measured data via rain sensor in tropical region," in *2022 IEEE 6th International Symposium on Telecommunication Technologies (ISTT)*, Nov. 2022, pp. 50–55, doi: 10.1109/ISTT56288.2022.9966549.
- [4] J. M. Riera, A. Benarroch, P. Garcia-del-Pino, and S. Perez-Pena, "Preprocessing and assessment of rain drop size distributions measured with a k-band doppler radar and an optical disdrometer," *IEEE Transactions on Instrumentation and Measurement*, vol. 70, pp. 1–8, 2021, doi: 10.1109/TIM.2020.3007909.
- [5] T.-S. Yee, P.-S. Kooi, M.-S. Leong, and L.-W. Li, "Tropical raindrop size distribution for the prediction of rain attenuation of microwaves in the 10-40 GHz band," *IEEE Transactions on Antennas and Propagation*, vol. 49, no. 1, pp. 80–83, 2001, doi: 10.1109/8.910533.
- [6] Y. Kim, J. Kim, J. Oh, Y. Yoon, S. Park, and J. Lee, "Rain attenuations based on drop size distribution (DSD) model and empirical model at low THz frequencies," *Electronics*, vol. 13, no. 1, Dec. 2023, doi: 10.3390/electronics13010009.
- [7] P. H. Ntanguen, A. Nzeukou Takougang, and A. T. Sandjon, "Raindrop size distribution and rainfall attenuation modeling from disdrometer measurement in central Africa: case of Cameroon," *Progress In Electromagnetics Research C*, vol. 121, pp. 243–253, 2022, doi: 10.2528/PIERC22052507.
- [8] J. M. Riera, A. Benarroch, P. Garcia-del-Pino, and S. Perez-Pena, "On the use of experimental drop size distributions from different instruments in millimeter-wave propagation studies," *IEEE Antennas and Wireless Propagation Letters*, vol. 20, no. 8, pp. 1384–1388, Aug. 2021, doi: 10.1109/LAWP.2021.3081376.
- [9] S. Das and A. R. Jameson, "Site diversity prediction at a tropical location from single-site rain measurements using a Bayesian technique," *Radio Science*, vol. 53, no. 6, pp. 830–844, Jun. 2018, doi: 10.1029/2018RS006597.
- [10] C. Han *et al.*, "Characteristics of rain-induced attenuation over signal links at frequency ranges of 25 and 38 GHz observed in Beijing," *Remote Sensing*, vol. 13, no. 11, May 2021, doi: 10.3390/rs13112156.
- [11] J. M. Riera *et al.*, "Characterization of rain attenuation in 80–200 GHz from experimental drop size distributions," *IEEE Transactions on Antennas and Propagation*, vol. 71, no. 5, pp. 4371–4379, May 2023, doi: 10.1109/TAP.2023.3259682.
- [12] Yagaseena, "Evaluation of two-part rain attenuation model at ku-band for tropical and equatorial regions," *Journal of Physics: Conference Series*, vol. 2312, no. 1, Aug. 2022, doi: 10.1088/1742-6596/2312/1/012004.
- [13] S. Nandi and D. Nandi, "Comparative study of rain attenuation effects for the design of 5G millimeter wave communication between tropical and temperate region," in *2017 Devices for Integrated Circuit (DevIC)*, Mar. 2017, vol. 26, pp. 747–750, doi: 10.1109/DEVIC.2017.8074051.
- [14] I. Joseph, I. H. Ojochogwu, and I. Odesanya, "Tropical rain intensity impact on raindrop diameter and specific signal attenuation at microwaves communication link," *International Journal of Image, Graphics and Signal Processing*, vol. 15, no. 2, pp. 59–72, Apr. 2023, doi: 10.5815/ijigsp.2023.02.06.
- [15] U. Mankong *et al.*, "Millimeter wave attenuation due to wind and heavy rain in a tropical region," *Sensors*, vol. 23, no. 5, Feb. 2023, doi: 10.3390/s23052532.
- [16] I. Mata-Alonso, J. M. Riera, L. Luini, H. Y. Lam, and D. Pimienta-del-Valle, "Rain attenuation at millimeter waves in different climatic zones estimated from drop size distributions," in *2024 18th European Conference on Antennas and Propagation (EuCAP)*, Mar. 2024, pp. 1–5, doi: 10.23919/EuCAP60739.2024.10501081.
- [17] A. De and A. Maitra, "Modeling of rain drop size distribution in association with convective and cloud parameter over a tropical location," *IEEE Transactions on Geoscience and Remote Sensing*, vol. 61, pp. 1–9, 2023, doi: 10.1109/TGRS.2023.3248664.
- [18] A. K. Verma, R. Nandan, and A. Verma, "Rain drop size distribution and variability of specific rain attenuation for Indian climate," in *2019 URSI Asia-Pacific Radio Science Conference (AP-RASC)*, Mar. 2019, vol. 25, pp. 1–4, doi: 10.23919/URSIAP-RASC.2019.8738722.
- [19] A. A. Alonge, "Semi-empirical characteristics of modified lognormal DSD inputs using rain rate distributions for radio links over the African continent," *Advances in Space Research*, vol. 67, no. 1, pp. 179–197, Jan. 2021, doi: 10.1016/j.asr.2020.09.017.
- [20] K. I. Timothy, J. T. Ong, and E. B. L. Choo, "Raindrop size distribution using method of moments for terrestrial and satellite

- communication applications in Singapore,” *IEEE Transactions on Antennas and Propagation*, vol. 50, no. 10, pp. 1420–1424, Oct. 2002, doi: 10.1109/TAP.2002.802091.
- [21] Disdrometer, “Disdrometer RD-80: user guide for disdrodata 2.0,” *Disdromet Ltd.*, 2009. <http://www.distromet.com> (accessed Jun. 20, 2022).
- [22] R. Gunn and G. D. Kinzer, “The terminal velocity of fall for water droplets in stagnant air,” *Journal of Meteorology*, vol. 6, no. 4, pp. 243–248, Aug. 1949, doi: 10.1175/1520-0469(1949)006<0243:TTVOFF>2.0.CO;2.
- [23] D. Atlas, R. C. Srivastava, and R. S. Sekhon, “Doppler radar characteristics of precipitation at vertical incidence,” *Reviews of Geophysics*, vol. 11, no. 1, pp. 1–35, Feb. 1973, doi: 10.1029/RG011i001p00001.
- [24] H. Y. Lam, J. Din, and S. L. Jong, “Statistical and physical descriptions of raindrop size distributions in equatorial Malaysia from disdrometer observations,” *Advances in Meteorology*, vol. 2015, pp. 1–14, 2015, doi: 10.1155/2015/253730.
- [25] A. M. Al-Saman, M. Cheffena, M. Mohamed, M. H. Azmi, and Y. Ai, “Statistical analysis of rain at millimeter waves in tropical area,” *IEEE Access*, vol. 8, pp. 51044–51061, 2020, doi: 10.1109/ACCESS.2020.2979683.
- [26] I. Shaye, T. Abd. Rahman, M. H. Azmi, and M. R. Islam, “Real measurement study for rain rate and rain attenuation conducted over 26 GHz microwave 5G link system in Malaysia,” *IEEE Access*, vol. 6, pp. 19044–19064, 2018, doi: 10.1109/ACCESS.2018.2810855.
- [27] S. N. A. S. Zafar, S. N. Hazmin, R. Mat, M. S. Marhamah, and R. Umar, “Wind speed on ultra high frequency (UHF) of radio signal,” *Journal of Fundamental and Applied Sciences*, vol. 10, no. 1S, pp. 278–287, 2018.
- [28] W. S. W. Nik, M. Z. Ibrahim, F. F. Ahmad, K. Samo, and A. M. Muzathik, “Wind energy potential at east coast of Peninsular Malaysia,” *International Journal of Applied Engineering Research, Dindigul*, vol. 2, no. 2, pp. 360–366, 2011.
- [29] S. Z. Satari, Y. Z. Zubairi, A. G. Hussin, and S. F. Hassan, “Some statistical characteristic of Malaysian wind direction recorded at maximum wind speed: 1999–2008,” *Sains Malaysiana*, vol. 44, no. 10, pp. 1521–1530, Oct. 2015, doi: 10.17576/jsm-2015-4410-18.
- [30] N. H. Zakaria, S. A. Salleh, A. Asmat, and M. A. Islam, “Seasonal windstorm pattern and damages in Peninsular Malaysia 2018,” *IOP Conference Series: Earth and Environmental Science*, vol. 385, no. 1, Nov. 2019, doi: 10.1088/1755-1315/385/1/012029.
- [31] N. H. Moslim, Y. Z. Zubairi, A. G. Hussin, S. F. Hassan, and N. A. Mokhtar, “Understanding the pattern of wind direction in Peninsular Malaysia,” *AIP Conference Proceedings*, vol. 2500. AIP Publishing, 2023, doi: 10.1063/5.0109944.
- [32] N. A. B. Kamisan, A. G. Hussin, and Y. Z. Zubairi, “Finding the best circular distribution for southwesterly monsoon wind direction in Malaysia,” *Sains Malaysiana*, vol. 39, no. 3, pp. 387–393, 2010.
- [33] K. J. Jang, Y. Yoon, J. Kim, J. H. Kim, and G. Hwang, “Rain attenuation prediction model for terrestrial links using gaussian process regression,” *IEEE Communications Letters*, vol. 25, no. 11, pp. 3719–3723, Nov. 2021, doi: 10.1109/LCOMM.2021.3109619.
- [34] ITU-R, “P.838: specific attenuation model for rain for use in prediction methods,” *ITU Radiocommunication Sector (ITU-R)*. 2005, Accessed: Nov. 04, 2021. [Online]. Available: <https://www.itu.int/rec/R-REC-P.838-3-200503-I/en>.
- [35] M. O. Ajewole, L. B. Kolawole, and G. O. Ajayi, “Cross polarization on line-of-sight links in a tropical location: effects of the variation in canting angle and rain dropsize distributions,” *IEEE Transactions on Antennas and Propagation*, vol. 47, no. 8, pp. 1254–1259, 1999, doi: 10.1109/8.791940.
- [36] T. Y. Kolade-Oje, M. O. Ajewole, J. S. Ojo, and A. T. Adediji, “Computation of spherical and non-spherical raindrop scattering parameters using the mie and T-matrix models in relation to 5G wireless systems,” *The European Physical Journal Plus*, vol. 137, no. 6, Jun. 2022, doi: 10.1140/epjp/s13360-022-02893-3.
- [37] W. Asen and T. Tjelta, “A novel method for predicting site dependent specific rain attenuation of millimeter radio waves,” *IEEE Transactions on Antennas and Propagation*, vol. 51, no. 10, pp. 2987–2999, Oct. 2003, doi: 10.1109/TAP.2003.818005.
- [38] J. Leinonen, “High-level interface to T-matrix scattering calculations: architecture, capabilities and limitations,” *Optics Express*, vol. 22, no. 2, Jan. 2014, doi: 10.1364/OE.22.001655.
- [39] K. Xizheng, Y. Lihong, and M. Dongdong, “Transmitted attenuation of laser signal in rain,” *Infrared and Laser Engineering*, vol. 37, no. 6, pp. 1021–1024, 2009.
- [40] O. Adetan and O. Obiyemi, “Analysis of raindrop diameters for rainfall attenuation in Southern Africa,” *International Journal of Electrical and Computer Engineering*, vol. 6, no. 1, p. 82, Feb. 2016, doi: 10.11591/ijece.v6i1.8746.
- [41] O. Adetan and O. Oludare Fagbohun, “Analytical approach to critical diameters in raindrop size distribution in Durban, South Africa,” *Asian Journal of Advanced Research and Reports*, pp. 1–8, Apr. 2018, doi: 10.9734/ajarr/2018/v1i113014.
- [42] O. Adetan and T. J. Afullo, “Raindrop size distribution and rainfall attenuation modeling in equatorial and subtropical Africa: the critical diameters,” *annals of telecommunications - annales des télécommunications*, vol. 69, no. 11–12, pp. 607–619, Dec. 2014, doi: 10.1007/s12243-013-0418-z.
- [43] L. Doherty and S. Stone, “Forward scatter from rain,” *IRE Transactions on Antennas and Propagation*, vol. 8, no. 4, pp. 414–418, Jul. 1960, doi: 10.1109/TAP.1960.1144879.
- [44] J. T. Hodges, G. Gréhan, G. Gouesbet, and C. Presser, “Forward scattering of a Gaussian beam by a nonabsorbing sphere,” *Applied Optics*, vol. 34, no. 12, Apr. 1995, doi: 10.1364/AO.34.002120.
- [45] M. Bennett, E. J. Kleczyk, K. Hayes, and R. Mehta, “Evaluating similarities and differences between machine learning and traditional statistical modeling in healthcare analytics,” *Artificial Intelligence*. IntechOpen, Dec. 2022, doi: 10.5772/intechopen.105116.
- [46] C. Wong, J. Liew, Z. Yusop, T. Ismail, R. Venneker, and S. Uhlenbrook, “Rainfall characteristics and regionalization in peninsular Malaysia based on a high resolution gridded data set,” *Water*, vol. 8, no. 11, Nov. 2016, doi: 10.3390/w8110500.
- [47] T. Narayana Rao, K. Amarjyothi, and S. V. B. Rao, “Attenuation relations for monsoonal rain at the X band from disdrometric measurements: Dependency on temperature, raindrop size distribution and drop shape models,” *Quarterly Journal of the Royal Meteorological Society*, vol. 144, no. S1, pp. 64–76, Nov. 2018, doi: 10.1002/qj.3291.
- [48] T. Kozu et al., “Seasonal and diurnal variations of raindrop size distribution in Asian monsoon region,” *Journal of the Meteorological Society of Japan. Ser. II*, vol. 84A, pp. 195–209, 2006, doi: 10.2151/jmsj.84a.195.
- [49] A. I. O. Yussuff, M. O. Ayeni, and O. E. Oreoluwa, “Adoption of deep neural network model for the prediction of rain attenuation,” *European Journal of Electrical Engineering and Computer Science*, vol. 7, no. 1, pp. 70–73, Feb. 2023, doi: 10.24018/ejece.2023.7.1.498.
- [50] J. S. Ojo, C. K. Ijomah, and S. B. Akinpelu, “Artificial neural networks for earth-space link applications: a prediction approach and intercomparison of rain-influenced attenuation models,” *International Journal of Intelligent Systems and Applications*, vol. 14, no. 5, pp. 47–58, Oct. 2022, doi: 10.5815/ijisa.2022.05.05.
- [51] A. Daher, H. Al Sakka, and A. K. Chaaban, “Low complexity single-layer neural network for enhanced rainfall estimation using microwave links,” *Journal of Hydroinformatics*, vol. 25, no. 1, pp. 101–112, Jan. 2023, doi: 10.2166/hydro.2022.099.




- [52] J. Polz, C. Chwala, M. Graf, and H. Kunstmann, "Rain event detection in commercial microwave link attenuation data using convolutional neural networks," *Atmospheric Measurement Techniques*, vol. 13, no. 7, pp. 3835–3853, Jul. 2020, doi: 10.5194/amt-13-3835-2020.
- [53] S. N. Livieratos and P. G. Cottis, "Rain attenuation along terrestrial millimeter wave links: a new prediction method based on supervised machine learning," *IEEE Access*, vol. 7, pp. 138745–138756, 2019, doi: 10.1109/ACCESS.2019.2939498.
- [54] M. Alhilali, J. Din, M. Schönhuber, and H. Y. Lam, "Estimation of millimeter wave attenuation due to rain using 2D video distrometer data in Malaysia," *Indonesian Journal of Electrical Engineering and Computer Science*, vol. 7, no. 1, pp. 164–169, Jul. 2017, doi: 10.11591/ijeecs.v7.i1.pp164-169.
- [55] H. Y. Lam, L. Luini, J. Din, M. J. Alhilali, S. L. Jong, and F. Cuervo, "Impact of rain attenuation on 5G millimeter wave communication systems in equatorial Malaysia investigated through disdrometer data," in *2017 11th European Conference on Antennas and Propagation (EuCAP)*, Mar. 2017, vol. 21, pp. 1793–1797, doi: 10.23919/EuCAP.2017.7928616.
- [56] U. A., "Simulation of different cloud attenuation methods," *2023 Second International Conference on Electrical, Electronics, Information and Communication Technologies (ICEEICT)*, vol. 20. IEEE, pp. 1–5, Apr. 2023, doi: 10.1109/ICEEICT56924.2023.10157966.
- [57] E. Regonesi, L. Luini, and C. Riva, "Limitations of the ITU-R P.838-3 model for rain specific attenuation," in *2019 13th European Conference on Antennas and Propagation (EuCAP)*, 2019, pp. 1–4.
- [58] A. A. Yusuf, A. Falade, B. J. Olufeagba, O. O. Mohammed, and T. A. Rahman, "Statistical evaluation of measured rain attenuation in tropical climate and comparison with prediction models," *Journal of Microwaves, Optoelectronics and Electromagnetic Applications*, vol. 15, no. 2, pp. 123–134, Jun. 2016, doi: 10.1590/2179-10742016v15i2624.
- [59] O. M. Adewusi, T. V. Omotosho, M. L. Akinyemi, S. A. Akinwumi, and O. O. Ometan, "Advancement on cloud attenuation modelling in tropical Ota climatic zone," *Journal of Physics: Conference Series*, vol. 1299, no. 1, Aug. 2019, doi: 10.1088/1742-6596/1299/1/012049.
- [60] E. Alozie *et al.*, "A review on rain signal attenuation modeling, analysis and validation techniques: advances, challenges and future direction," *Sustainability*, vol. 14, no. 18, Sep. 2022, doi: 10.3390/su141811744.

## BIOGRAPHIES OF AUTHORS






**Nurul Najwa Md Yusof**    is a Ph.D. candidate at the Faculty of Electrical Engineering, Universiti Teknologi Malaysia (UTM). She is also a senior lecturer under the Polytechnic and Community College Education Department (JPPKK), Ministry of Higher Education. She received her B.Eng. in electrical engineering (information technology) and masters of technical and vocational education (TVET) from Institute Teknologi Tun Hussein Onn Malaysia currently known as Tun Hussein Onn University of Malaysia (UTHM). She also holds a M.Eng. in electronic engineering (telecommunication systems) from Universiti Teknikal Melaka Malaysia (UTEM). She is a graduate member of Board of Engineers Malaysia (BEM) and student member of IEEE. Her research interests include radio wave propagation, satellite and terrestrial communications, fiber optic communication systems and TVET. She can be contacted via email: awa.md.yusof@gmail.com.



**Jafri Din**    is a distinguished expert in radio wave propagation, satellite technology, HAPS, TV broadcasting, weather radar, acoustic fisheries techniques, and satellite communications. He received the B.Sc. degree in electrical engineering from Tri-State University, Angola, in USA, in 1988, and the Ph.D. degree from the Universiti Teknologi Malaysia (UTM), Johor, Malaysia, in 1997. From 2008 to 2015, he was the Head of Departments, Undergraduate Academic Manager, and the Deputy Dean (Development) of the Faculty of Electrical Engineering (FKE), UTM. He has also served as the Director of the wireless communication center, UTM. Currently he is the Dean of the faculty from November 2022. He can be contacted via email: jafri@utm.my.



**Lam Hong Yin**    received the M. Eng. and Ph.D. degrees in electrical engineering from the Universiti Teknologi Malaysia (UTM), Johor, Malaysia, in 2009 and 2013, respectively. Currently, he is the head of the electrical engineering technology Department at Pagoh Campus. Lam is a graduate member of BEM, registered Professional Technologist MBOT, Member of IEEE, and American Association for the Advancement of Science. He serves as a reviewer for various international journals such as IEEE Transactions on Antennas & Propagation and IEEE Antennas and Propagation Magazine. Besides research activities, he is also actively involved as an Engineering Technology Accreditation Council and MBOT academic program evaluation panel, as well as a quality assurance audit ISO 9001:2015 lead auditor. His research interests include weather radar technology, radio wave propagation, satellite and terrestrial communication and atmospheric sciences. He can be contacted via email: hylam@uthm.edu.my.